Accepted Manuscript

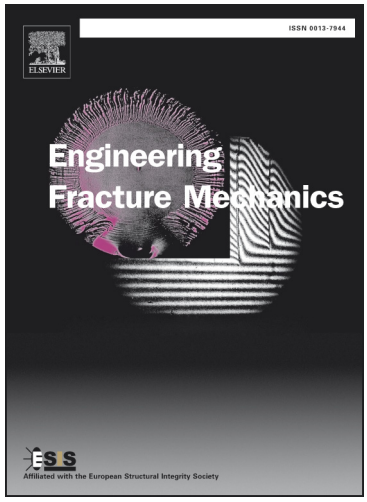

Constraint analysis of defects in strength mismatched girth welds of (pressurized) pipe and curved wide plate tensile test specimens

M.A. Verstraete, W. De Waele, R.M. Denys, K. Van Minnebruggen, S. Hertelé

PII: S0013-7944(14)00228-8
DOI: http://dx.doi.org/10.1016/j.engfracmech.2014.07.018
Reference: EFM 4339

To appear in: *Engineering Fracture Mechanics*

Received Date: 11 October 2012
Revised Date: 11 May 2014
Accepted Date: 18 July 2014

Please cite this article as: Verstraete, M.A., De Waele, W., Denys, R.M., Van Minnebruggen, K., Hertelé, S., Constraint analysis of defects in strength mismatched girth welds of (pressurized) pipe and curved wide plate tensile test specimens, *Engineering Fracture Mechanics* (2014), doi: http://dx.doi.org/10.1016/j.engfracmech.2014.07.018

Constraint analysis of defects in strength mismatched girth welds of (pressurized) pipe and curved wide plate tensile test specimens

M.A. Verstraete[a,*], W. De Waele[a], R.M. Denys[a], K. Van Minnebruggen[a], S. Hertelé[a]

[a]Ghent University, Department of Mechanical Construction and Production, Soete Laboratory, Technologiepark gebouw 903, 9052 Zwijnaarde, Belgium
*Corresponding author: Matthias.Verstraete@UGent.be

Abstract: (max 100 words)

Curved Wide Plate (CWP) specimens are often considered to evaluate the tensile strain capacity of girth weld defected pipelines. However, to date no comparison has been made between the constraint in CWP and (pressurized) pipe specimens. This paper reports on the evaluation of the constraint through three dimensional finite element simulations. At first, it is observed that the internal pressure marginally increases the out-of-plane constraint. Second, the CWP specimens appear to closely represent the constraint in pipe specimens for homogeneous as well as strength mismatched situations. CWP specimens become increasingly conservative to pipe specimens with increasing defect dimensions.

Keywords: (to be selected from list made available by Elsevier)

Constraint effects
J-integral
Plasticity

1. Introduction

Transportation pipelines installed in harsh environments might be subjected to displacement controlled loading during operation (e.g. due to landslides). This might result in large (plastic) deformations. The girth welds that connect different pipes unavoidably contain defects, not all of which can be repaired for economical reasons. Accordingly, an assessment procedure is required to determine the allowable defect sizes and/or tensile strain capacity. The determination of these limits can be performed by means of full scale testing. Next to axial tension these tests should incorporate internal pressure, as the resulting biaxial loading condition is known to be strongly detrimental to crack driving force [1, 2]. However, such tests require high test capacities and are time consuming.

Alternatively, sub-scale test specimens can be considered. Since the 1980's, Curved Wide Plate (CWP) testing has been widely used to assess defected girth welds [3-5]. However, these tests do not reflect the actual geometry nor the loading conditions; with the main drawback that internal pressure is lacking. Nevertheless, application of a so-called pressure correction factor allows estimation of the tensile strain capacity for full scale pipes using the results of CWP testing [6-8]. Such correction however implicitly assumes that the apparent toughness is comparable in both CWP and (pressurized) pipe specimens.

To verify the assumption with respect to the apparent toughness, this study evaluates the stresses ahead of the crack tip based on an extensive set of three dimensional finite element simulations. These stresses are known to influence the apparent toughness due to the constraint developing ahead of the crack tip. Several theoretical frameworks are available to characterize this constraint level [9-11]. In this study a constraint analysis is carried out based on the two-parameter *J-Q* framework developed by

Shih and O'Dowd in the early 1990's [12, 13], which is well accepted for situations with pronounced plasticity [14]. In addition, the stress triaxiality parameter h, defined as the ratio between the hydrostatic stress and Von Mises equivalent stress, is evaluated ahead of the crack tip [15, 16]. The equivalence between the constraint parameters Q and h has been reported in literature [17, 18], though the stress triaxiality is assumed to have a higher physical relevance in case of ductile failure. These constraint analyses are first performed for homogeneous specimens. Subsequently, the influence of weld strength mismatch is considered, as strength overmatching welds are generally required for plastically deforming pipelines.

The remainder of this paper is structured as follows; first, a description of the test specimen geometries and finite element models is provided in paragraph 3. Second, in paragraph 4 an evaluation is made of the constraint evolution in (pressurized) pipes and CWP specimens. Conclusions are given in paragraph 5.

2. Nomenclature

a	defect depth
b_0	initial remaining ligament thickness
c	half defect arc length
D	pipe diameter
E	Young's modulus
h	stress triaxiality
J	J-integral
n	strain hardening exponent
Q	constraint parameter (uniaxial)
Q_m	constraint parameter (triaxial)
ΔQ	variation of Q-parameter
$\bar{r}$	normalized distance ahead of the crack tip
t	pipe wall thickness
Y/T	yield-to-tensile ratio
ε	true strain
θ	angle perpendicular to the crack
•	angle parallel to the crack
σ	true stress
σ_0	yield strength
σ_e	Von Mises equivalent stress
σ_{hoop}	hoop stress
σ_{ij}	stress in ij-direction
σ_m	hydrostatic stress
$\%MM$	yield strength mismatch

3. Methodology

This paragraph provides a description of the simulated test specimen geometries. Second, the developed finite element models and associated assumptions are outlined. The third subsection elaborates on material properties and simulation of weld strength mismatched configurations. The final subsection provides a brief description of the constraint calculations presented in this paper.

3.1. Geometry of Curved Wide Plate and pipe specimens

The simulated pipe specimens are characterized by their outer diameter (D) and wall thickness (t) (Figure 1a). Within the set of simulations performed, the wall thickness was fixed at 15 mm. The diameter is varied between 762 mm (30") and 1270 mm (50"). The length of the simulated pipe specimens equals four times their diameter, which suffices to yield results independent from the boundary conditions [19].

In practice, CWP specimens are extracted from pipe specimens. Accordingly, these have a curvature defined by the pipe's diameter and have the same wall thickness. The total length of the CWP specimens equals 1200 mm, whereas the prismatic section is 900 mm long and 300 mm wide (Figure 1b). All other geometrical properties are in agreement with the UGent Guidelines for CWP testing [3].

The specimens have constant depth surface breaking defects with an end-radius equal to the defect depth. The crack geometry is furthermore characterized by the defect depth (a) and defect arc length ($2c$). Unless otherwise specified, these defects are located at the weld metal centre along the pipe's inner diameter. The length has been varied between 25 mm and 100 mm. The depth of the crack varied between 3.0 and 6.0 mm, reflecting relative crack depths a/t between 0.20 and 0.40.

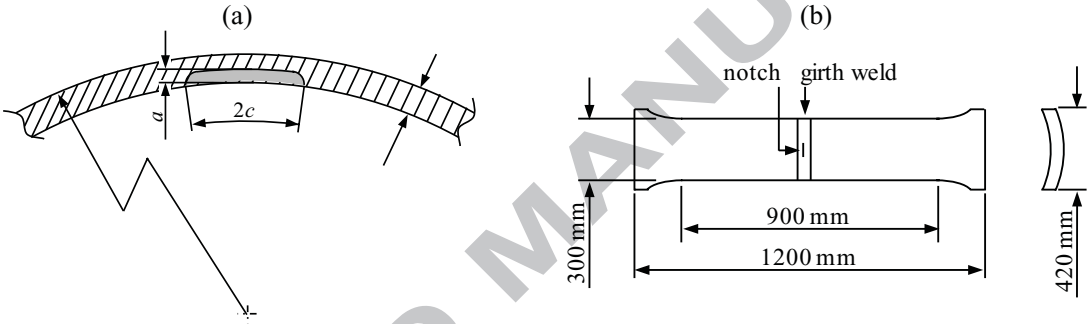

Figure 1: Definition of geometrical parameters: pipe (a) and CWP specimen (b)

3.2. Finite element models

Python™ scripts have been used to facilitate the parametric analysis of the above geometries through finite element simulations in Abaqus® v6.11. These scripts automatically generate, mesh, analyze and post-process the different geometries. For a detailed description of this scripting approach, the reader is referred to [20]. A main advantage hereof is the consistent mesh design, in particular around the crack tip. Regardless the dimensions of the crack and/or specimen, a gradually coarsening spider web mesh is created around the crack. This crack is initially blunted with an initial root radius of 2.5 µm. This radius is small enough to accurately represent an infinitely sharp crack [21]. A typical mesh design is shown in Figure 2. Note that only half of the specimens are modeled, symmetry boundary conditions being applied along the length of the specimens. Based on linear brick elements with reduced integration (Abaqus® type C3D8R), the resulting models consist of typically 80 000 and 35 000 nodes for pipe and CWP specimens respectively.

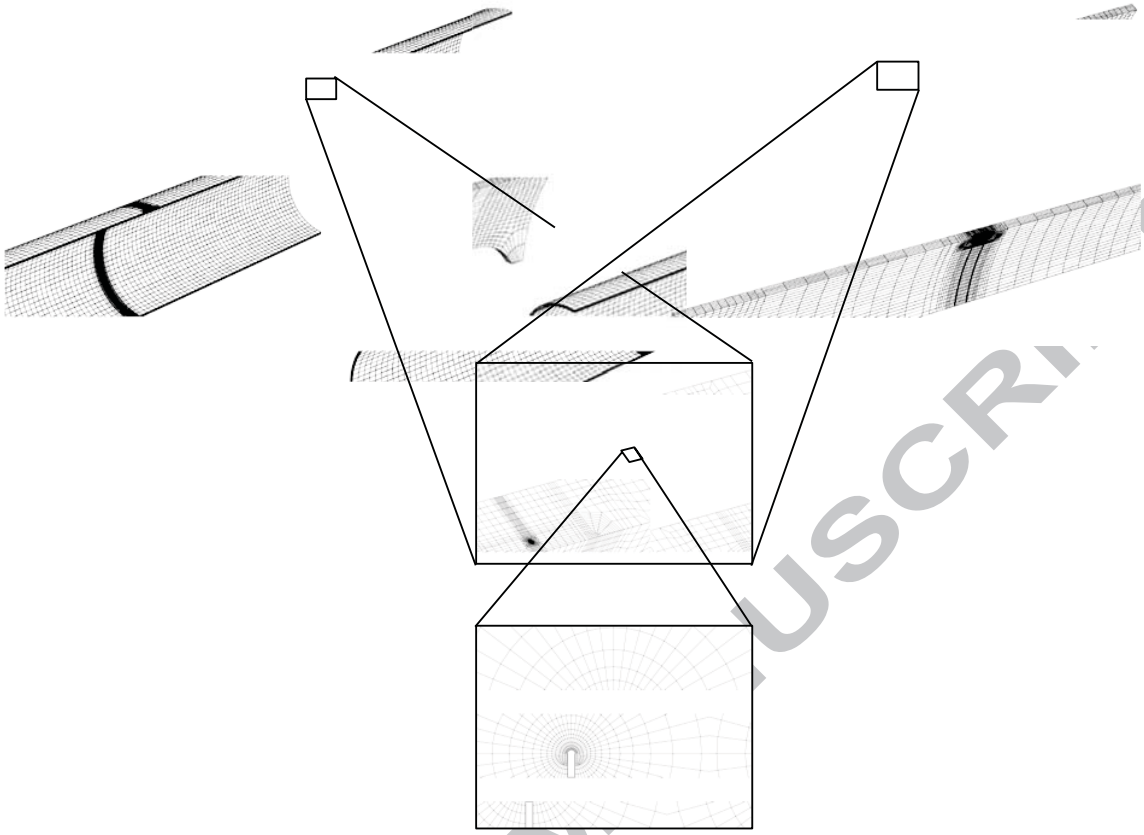

Figure 2: Characteristic mesh design for pipe specimens and CWP specimens

Next to the symmetry boundary conditions, displacement boundary conditions are applied representing the axial straining for both pipe and CWP specimens. Clamped boundary conditions are simulated, since a uniaxial, longitudinal displacement is imposed not allowing for any rotation. These displacements are transferred to the specimen through rigid bodies attached to the end of the specimen. In addition to the resulting axial load, the pipe specimens can be subjected to internal pressure. This pressure is applied at the inner diameter surface prior to the axial straining. For the simulated defects that are located at the inner diameter side, the internal pressure is also applied on the crack faces and tip. Simulations with and without additional pressure have been performed for comparison. In case of outer diameter defects, the internal pressure only acts on the pipe's inner diameter. Unless specifically mentioned, the pressure level (p) considered in this paper corresponds to a hoop stress (σ_{hoop}) equal to 80% of the pipe's actual yield strength.

The reference stress fields, required for the J-Q analyses (§3.5), are obtained from a Modified Boundary Layer (MBL) model with similar mesh design around the crack tip. These stress fields are evaluated at a fixed load level of $J = 50$ N/mm, defined by the load applied on the boundaries of the MBL model. This load level assures that the stress data are independent of the initial blunting [22].

3.3. Material properties and analysis approach

The analyses are completed using small strain assumptions. Although this is known to be an approximation, this approach has proven to yield a sufficiently accurate description of the crack tip stress fields [23]. In addition, this approach allows simulating weld metal strength overmatched configurations at high load levels in terms of J-integral, without observing a necking phenomenon in

the lower strength base material. Both for homogeneous and weld strength mismatched configurations, a non-linear elastic Ramberg-Osgood material model (i.e. deformation plasticity) is considered [24]. This model describes the true stress – true strain behavior based on the strain hardening exponent n, Young's modulus E and 0.2% proof stress σ_0, which serves as the yield strength. Within the framework of this study, a yield strength of 420 MPa and Young's modulus of 206980 MPa are considered. The strain hardening exponent is varied between $n = 5$ and $n = 20$, representing yield-to-tensile (Y/T) ratios between 0.46 and 0.90 respectively. It is noted that a Y/T-ratio of 0.46 is not realistic, however this case is considered to cover a wide area of applicability.

$$\varepsilon = \frac{\sigma}{E} + 0.002\left(\frac{\sigma}{\sigma_0}\right)^n \tag{1}$$

It should be noted that a non-linear elastic material definition was selected to enhance the convergence of the J-integral calculations, which are based on the domain integral method implemented in Abaqus®. A total of twelve contours are considered. In case of welded specimens, it is noted that all contours are contained within the weld metal region.

3.4. Simulated weld properties

For the analysis of weld strength mismatched situations, the mismatch level *(%MM)* is defined as the relative difference between the yield strength of the weld and base metal.

$$\%MM = \frac{\sigma_{0;WM} - \sigma_{0;BM}}{\sigma_{0;BM}} \cdot 100 \tag{2}$$

Within this paper, the difference between weld and base material solely originates from a difference in yield strength; the strain hardening exponents of weld and base material are identical. Yield strength mismatch levels are varied between -20% (strength undermatching weld) and +50% (strength overmatching weld) in steps of 10%. Two types of welds are analyzed based on the CSA recommendations for pipeline girth welding [25]. The first type aims to represent a manual weld with a wide V-shaped bevel preparation. Its opening angle equals 30° (Figure 3a). The second type reflects a narrow gap automated weld with weld bevel opening angle equal to 10° (Figure 3b). Both have a root opening of 5.0 mm. A weld cap reinforcement is modeled. This semi circular geometrical reinforcement has a height of 1.0 mm for both weld types. The weld bevel profile and weld cap reinforcement are modeled through application of nodal coordinate transformations [20]. It should be noted that only cracks located at the weld metal centre line are considered.

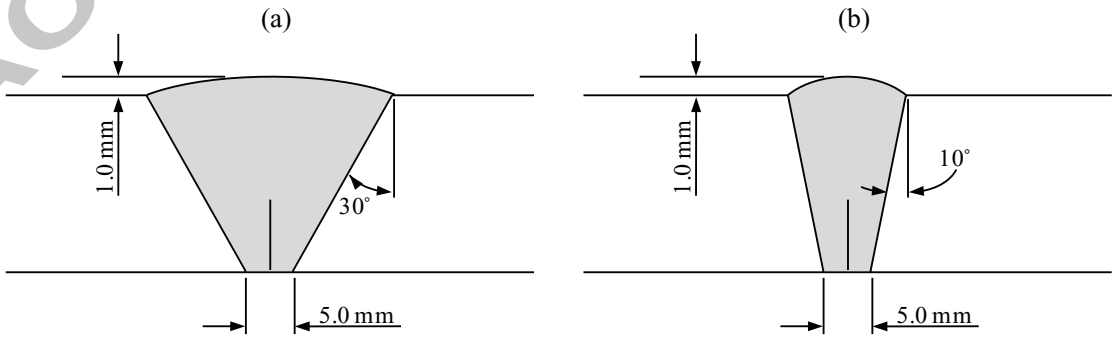

Figure 3: Investigated weld bevel geometries: wide V-shaped bevel (a) and narrow gap bevel (b)

3.5. Constraint calculations

First, the considered two-parameter *J*-*Q* framework is summarized [12, 13]. Within this framework, the *J*-integral is assumed to set the size of the plastic zone. Therefore, the distances ahead of the crack tip (*r*, Figure 4) are normalized by J/σ_0, with σ_0 the yield strength of the material where the crack is located (i.e. the weld metal's yield strength). Within this paper, the stress fields are examined at normalized distances $1 \le \bar{r} = r/(J/\sigma_0) \le 5$; this zone is believed to be significant for both ductile and brittle type fractures [26]. The second parameter, *Q*, determines a hydrostatic shift relative to a reference field ($\sigma_{ij;ref}$). This reference field is obtained from a Modified Boundary Layer (MBL) analysis. Both plane strain and plane stress MBL analyses have been carried out to select the most appropriate reference field. The material properties considered for this MBL model match those of the zone containing the crack (i.e. the weld metal for welded specimens). The *Q*-parameter is evaluated at a normalized distance of two ahead of the crack tip ($\theta = 90°$, Figure 4), in the forward region.

$$Q = \frac{\sigma_{\theta\theta} - \sigma_{\theta\theta;ref}}{\sigma_0} \qquad \bar{r} = r/(J/\sigma_0) = 2 \qquad \theta = 90° \tag{3}$$

Furthermore, both the middle of the crack (• = 0) and the surface ends of the crack (approx. • = *90*°) are considered. The middle of the crack is known to exhibit the highest crack driving force for long and shallow defects and is therefore believed to govern fracture [27]..

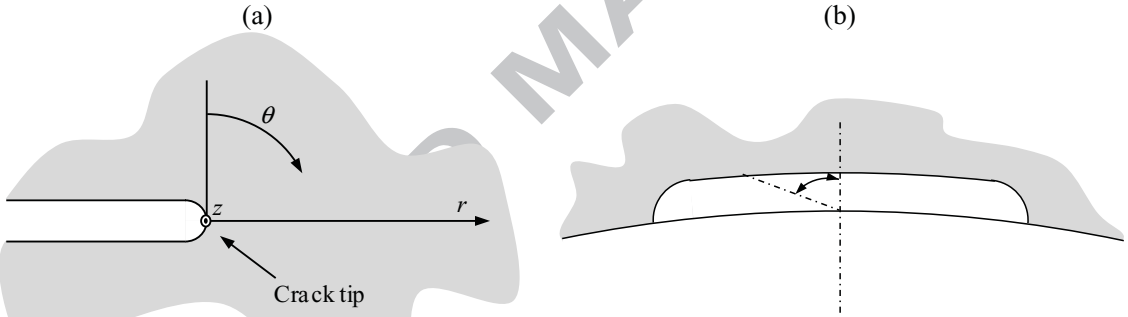

Figure 4: Definition of location relative to crack tip (a) and along crack front (b)

As the aim is to describe situations of ductile fracture behavior, the out-of-plane stress is well known to impact failure. Therefore, a second constraint parameter is evaluated that accounts for out-of-plane stresses, namely the Q_m-parameter. This parameter is based on the hydrostatic stress ahead of the crack tip and therefore more consistent with the interpretation as a triaxiality parameter [28].

$$Q_m = \frac{\sigma_m - \sigma_{m;ref}}{\sigma_0} \qquad \bar{r} = r/(J/\sigma_0) = 2 \qquad \theta = \pi/2 \tag{4}$$

The hydrostatic stress is defined as:

$$\sigma_m = \frac{\sigma_{ii}}{3} \tag{5}$$

In general both Q and Q_m yield similar values [28, 29], although Q_m is known to capture out-of-plane constraint effects more sensitively. The validity of the Q calculations is checked by evaluating the parallelism between the reference stress field obtained from a MBL model and the actual crack tip stress field. This is commonly performed through a comparison of the Q-parameters calculated at normalized distances ahead of the crack tip $\bar{r}=1$ and at $\bar{r}=5$ [30, 31].

$$\Delta Q = \frac{\left| Q_{\bar{r}=1} - Q_{\bar{r}=5} \right|}{4} \tag{6}$$

In accordance with results published in literature, this difference should be smaller than 0.1 to obtain a description of the crack tip stress fields whose accuracy is independent of the radial distance from the crack tip [14, 32]. High ΔQ values originate for instance from local bending stresses.

The third constraint parameter considered in this paper is the stress triaxiality parameter h. This parameter is defined as the ratio between the hydrostatic stress and the Von Mises equivalent stress. It is evaluated at the same locations as the Q-parameter.

$$h = \frac{\sigma_m}{\sigma_e} \qquad \bar{r} = r/(J/\sigma_0) = 2 \quad \theta = \pi/2 \tag{7}$$

Within this paper, only Q-values will be reported unless significant differences between different constraint parameters have been observed. Eventually, a comparison between the different constraint parameters is also presented.

4. Results and discussion

Within the following subsections the influence of different parameters (e.g. crack depth) on the evolution of the constraint ahead of the crack tip is discussed. These analyses are carried out on pressurized and unpressurized pipes and on CWP specimens. Representative results are shown for the sake of clarity, exceptions are explicitly highlighted. In all cases, the constraint is evaluated up to $J/\bullet_0$-values equal to two. For these values, remote plastic straining is clearly obtained. By means of example, the evolution of $J/\bullet_0$ is shown as function of the strain remote from the cracked ligament for a CWP and a pipe specimen (Figure 5).

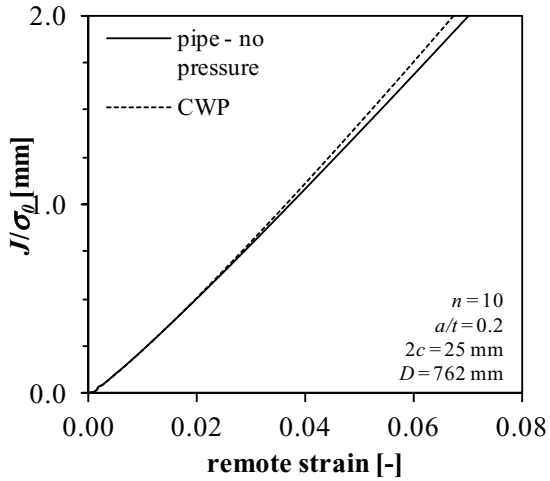

Figure 5: Example crack driving force curves for CWP and pipe specimens

4.1. Selection of reference stress field

The crack tip constraint is studied at both the middle of the crack and at the surface end of the crack. For these locations, the validity of the *J-Q* theory is checked based on the magnitude of the ΔQ values. Two types of reference fields have been considered in this paper, namely the plane strain and plane stress fields obtained from MBL analyses. These fields differ both in magnitude and in shape (Figure 6). The plane stress reference field has a lower magnitude and appears flatter as function of the normalized distance ahead of the crack tip. Consequently, the plane strain solution represents a higher constraint condition.

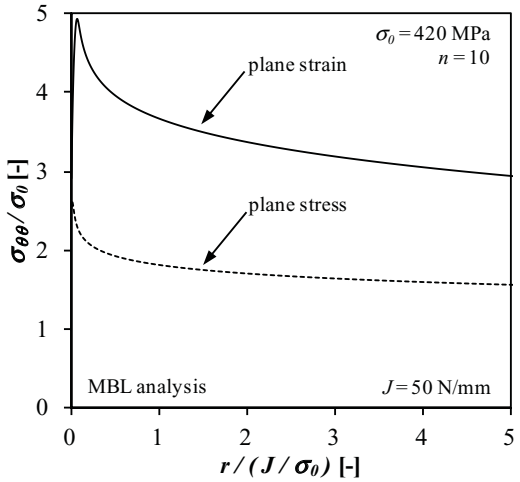

Figure 6: Plane stress and plane strain crack tip stress fields obtained from MBL analysis

First, the ΔQ values are calculated for the crack tip stress fields at the middle of the crack for pipe specimens (• = 0°). Considering the plane stress crack tip stress field as a reference field, the ΔQ values clearly exceed the critical value of 0.1 (Figure 7a). This implies that the actual crack tip stress fields are not parallel to the reference crack tip stress field. In contrast, when considering the plane strain solution for the reference stress field, the ΔQ values remain limited for almost all loading levels. Only at very low load levels, the ΔQ values exceed the critical value of 0.1, attributed to the initial crack tip blunting. Second, the crack tip stress fields at the surface end of the crack are studied (• • 90°). In this case, only the plane stress reference stress field results in ΔQ values below 0.1 (Figure 7b). As a result, the $Q_{(m)}$ values reported in the remainder of this paper are, unless explicitly specified otherwise, defined relative to the plane strain solution for the middle of the crack and the plane stress solution for the surface ends of the crack.

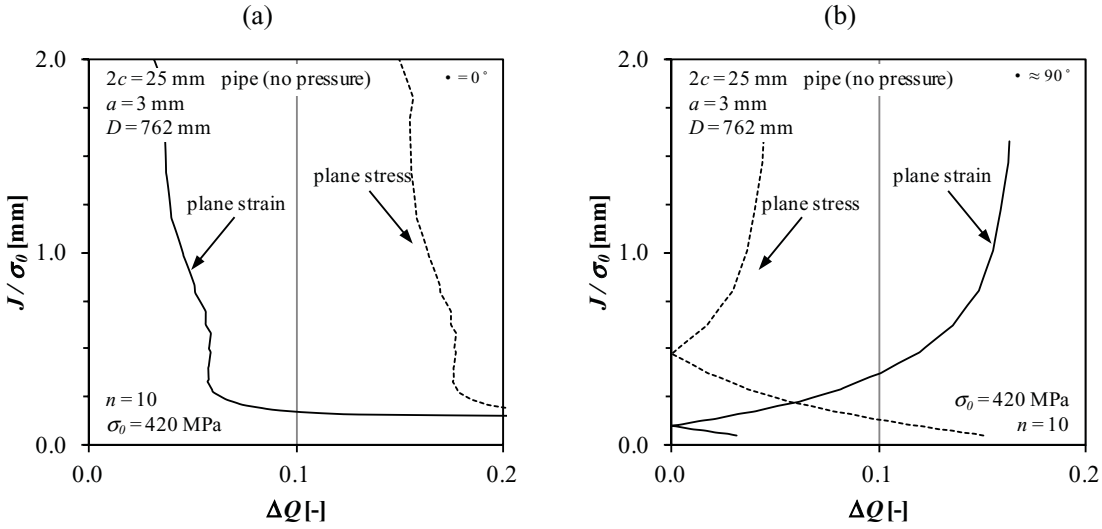

Figure 7: Calculated ΔQ values for plane strain and plane stress reference stress field at middle of the crack (a) and at surface ends of the crack (b)

To accommodate a comparison between these locations, the constraint at both locations is calculated relative to the same reference field, i.e. the plane strain reference stress field. As a result, the J Q trajectory for the surface end point of the crack is shifted compared to the situation using a plane stress reference stress field (Figure 8a). Relative to the constraint at the surface end of the crack, the constraint at the middle of the crack is higher. This observation is additionally supported by the evolution of the triaxiality parameter (Figure 8b). Similar observations have been made for all studied defects. Given the lower crack driving force at this location along the crack front, the occurrence of ductile crack extension in the circumferential direction is thus unlikely to occur for these defects. This corresponds well with the experimental observations of uniaxially loaded part-through defects [33].

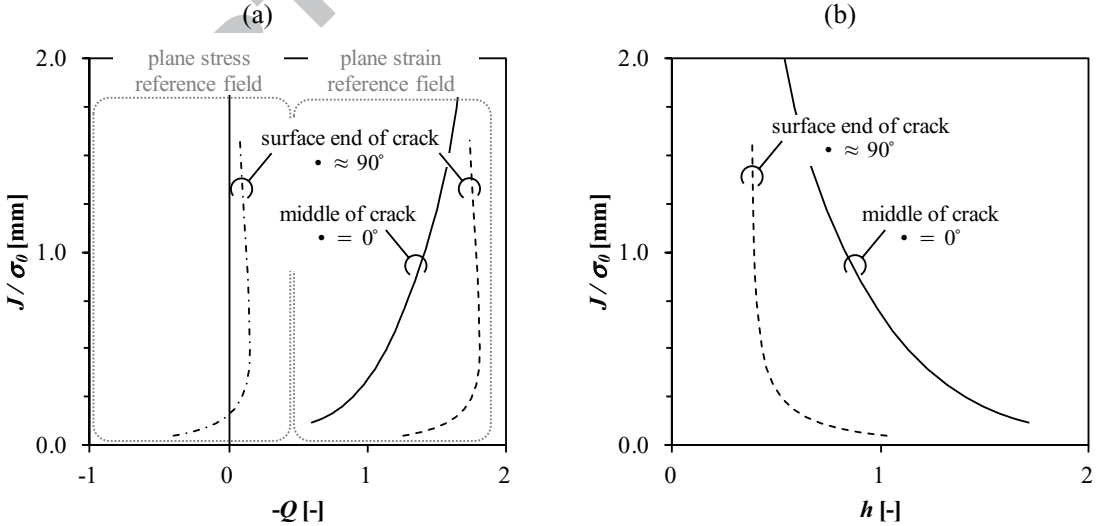

Figure 8: Constraint at surface ends of the crack and center of the crack based on Q-parameter and plane strain reference stress field (a) and triaxiality parameter h (b)

4.2. Influence of internal pressure

The internal pressure effect was studied both at the middle of the crack and at the end of the crack front near the free surface. First, the focus is at the middle of the crack. Looking at the resulting *J*-*Q* trajectories, no significant differences are observed between the various internal pressure levels (Figure 9a); all show a similar loss of constraint upon the development of plasticity. Therefore, it is concluded that, regarding the in-plane constraint, the degree of biaxiality in the loading situation has no influence.

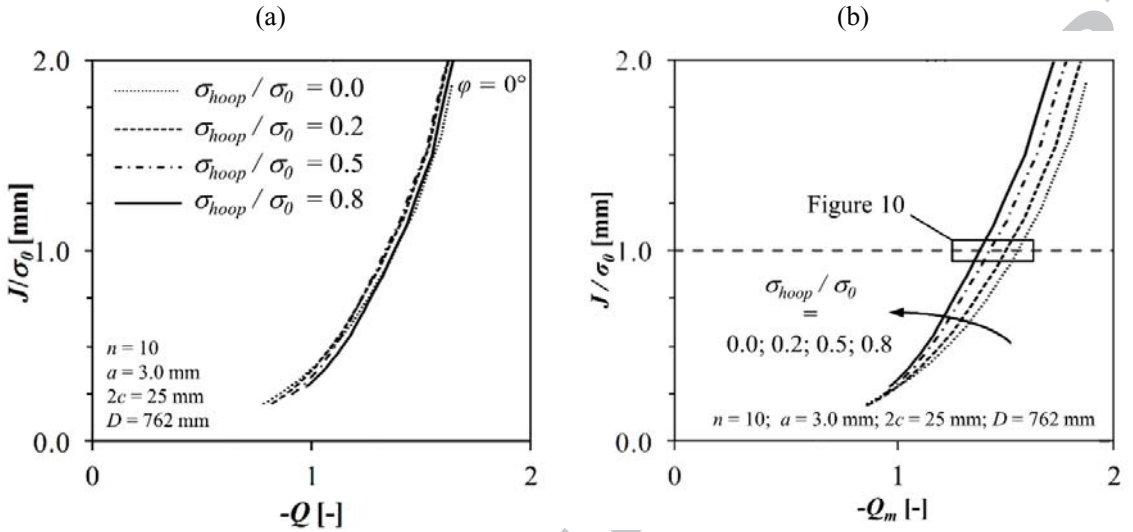

Figure 9: Resulting *J*-*Q* (a) and *J*-Q_m (b) trajectories for varying internal pressure levels

In contrast, when the out-of-plane constraint is more explicitly accounted for, e.g. by using the constraint parameter Q_m, a clear increase of the constraint is observed as the pressure level increases (Figure 9b). In Figure 10 the different constraint parameters are evaluated at a fixed crack driving force level (i.e. $J / \sigma_0 = 1$), for varying internal pressure levels. Regardless the considered material, the constraint increase appears approximately linearly proportional to the internal pressure level when taking into account the out-of-plane constraint. This finding somewhat contrasts with results published by Cravero et al. [34]. They have evaluated the triaxiality ahead of the crack tip for various pressure levels and concluded that no significant differences were observed. To the authors' experience only relatively low load levels were considered in their study, resulting in remarkable scatter due to initial blunting. On the other hand, these observations are in agreement with the results of Bass et al. [35], who also reported that the out-of-plane constraint is influenced by the biaxial loading level in contrast to the in-plane constraint.

Elaborating on the influence of the hoop stress, the influence of the flaw location is examined. Inner diameter defects differ from outer diameter defects as for the latter the pressure is not acting on the crack faces. No significant difference is observed between the (out-of-plane) constraint evolution for both defect locations (Figure 11a). This suggests that pressure acting on the crack faces does not influence the constraint. This is confirmed by comparing simulations for internal diameter cracks with and without pressure being applied on the crack faces (Figure 11b). Accordingly, the influence of internal pressure relates to the hoop stress rather than additional longitudinal or radial stress components.

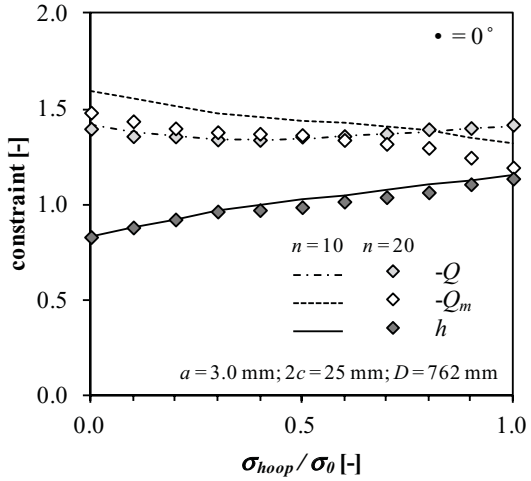

Figure 10: Influence of internal pressure on constraint parameters at middle of the crack

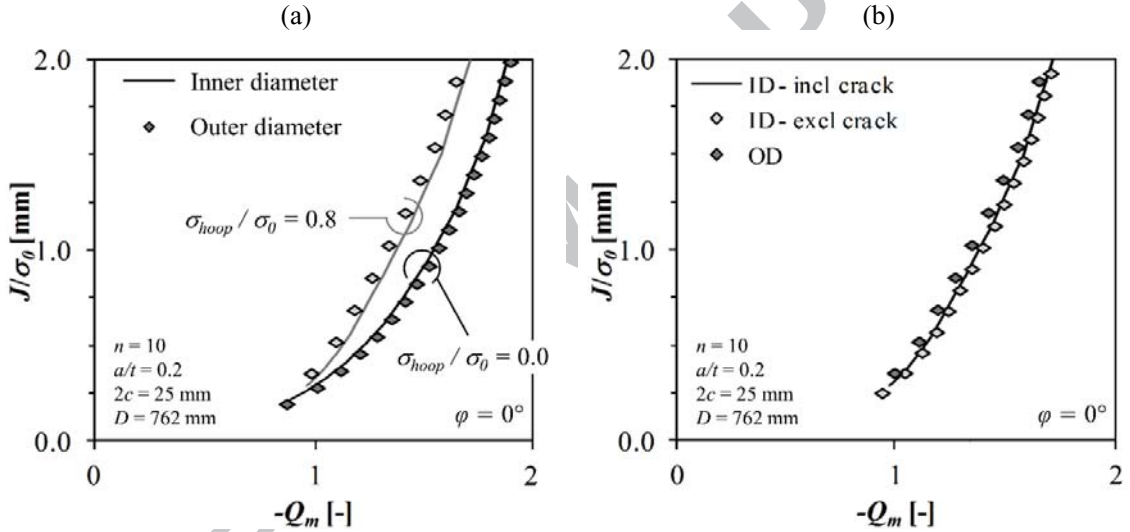

Figure 11: Influence of internal pressure on out-of-plane constraint:
comparison of defect location (a) and influence of pressure applied to the crack faces (b)

Second, the constraint is studied at the surface ends of the crack. Here, the Q-parameter again shows a limited dependency on the internal pressure level. In contrast, the parameters that explicitly account for the out-of-plane constraint, Q_m and h, indicate an increase of the constraint with increase of the internal pressure level (Figure 12). The magnitude of this constraint increase is comparable to the one observed at the middle of the crack, hence no additional crack extension in the circumferential direction is expected based on these constraint considerations.

Focusing on the current results, the observed effect can be explained by noting that, with increasing internal pressure, the hoop stresses increase. Hence, the out-of-plane stresses gain importance, resulting in higher Q_m and h values. Remark that this effect is not necessarily captured by Q, as this parameter only accounts for hoop stresses via the Poisson effect. This effect is of a secondary nature and may be within the accuracy range of the finite element calculations. Focusing on ductile fracture, the Q_m and h parameters are however believed to be more relevant, in contrast to cleavage where the in-plane constraint is of major importance [36]. Accordingly, the resistance curves of pressurized pipes

are expected to be lower than those obtained from unpressurized pipes. However, based on available literature reportings on both experimental and numerical work, only a minor decrease is observed in the *J-R* curve [37, 38]. This difference is most likely attributed to the limitations of the considered modeling approach. The constraint level in this paper was not studied inside the large deformation zone just in front of the crack tip. The small strain assumption made does not allow for investigations of this feature. In addition, a potential minor decrease can be neglected as scatter in the material properties is likely to influence the resistance curves more significantly [39]. Hence, it is concluded that the internal pressure increases the constraint, but to an extent that can be questioned to be relevant as scatter from material testing is likely to influence the obtained tearing resistance approximately to the same extent.

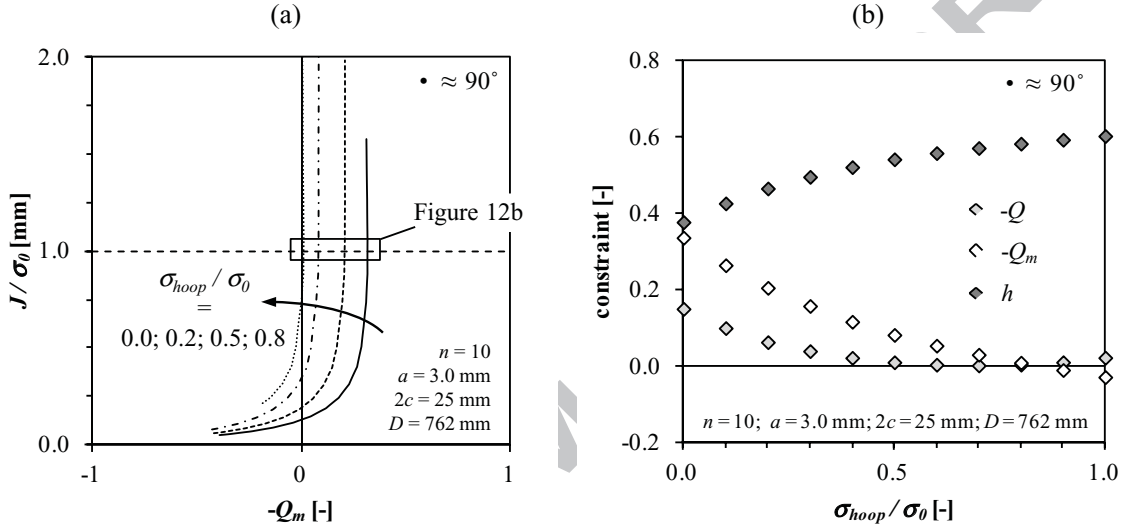

Figure 12: Influence of internal pressure on constraint parameter at surface end of crack (a) with detailed evolution at fixed loading level of $J / \bullet_0 = 1.0$ (b)

4.3. Influence of curved wide plate geometry

Comparing the constraint evolutions in CWP specimens and unpressurized pipes at the middle of the crack, it is clear that both show a similar loss of constraint upon loading (Figure 13). This statement holds particularly for small defects (a x $2c$ = 3.0 x 25 mm²). With increasing defect dimensions, the difference between CWP and pipe specimens increases, regardless the considered constraint definition. Shown in Figure 13a and b is the influence of the relative crack depth on the *J-Q* and *J-h* trajectory respectively. For shallow cracks ($a/t = 0.2$) the difference between pipe and CWP specimens is limited. In contrast, deep cracks ($a/t = 0.4$) indicate a higher constraint in the CWP specimens, in particular at lower load levels. Given the similarity between the trends described by the different constraint parameters, solely the *Q*-parameter will be considered in the remaining comparisons between pipe and CWP specimens. It is furthermore observed that the constraint increases for CWP specimens with increasing crack lengths (Figure 13c). This contrasts with the unpressurized pipe specimens, which show no dependence of the constraint trajectories on crack length.

Another factor potentially influencing the constraint in the CWP specimen is the pipe diameter. It is observed that CWP specimens extracted from larger diameter pipes show an increased raise of the constraint during the early loading stages (Figure 13d). In contrast, the constraint evolution in pipe specimens appears to be independent of diameter.

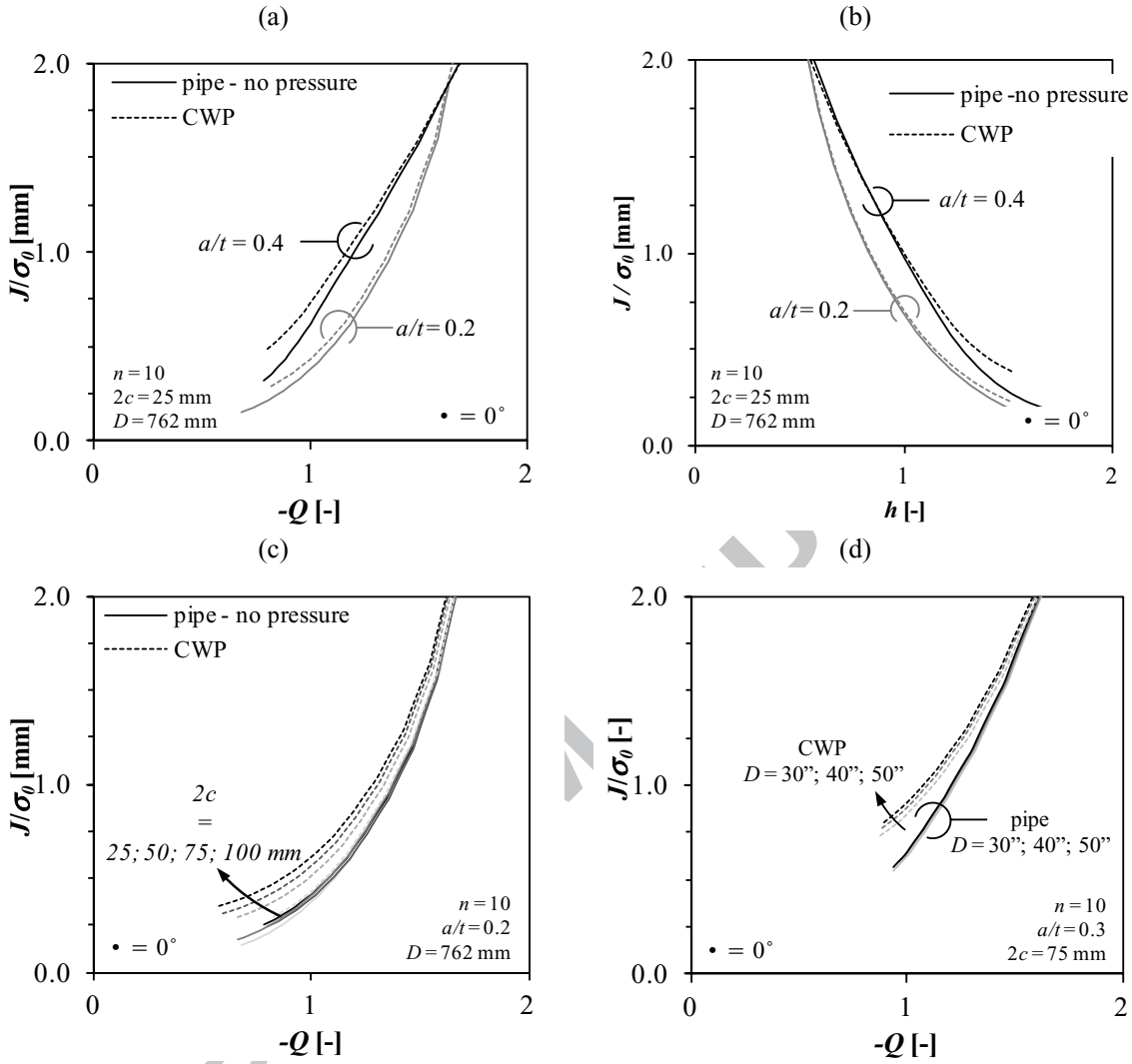

Figure 13: Influence of geometrical parameters on constraint in unpressurized pipe and CWP specimen: influence of relative crack depth on *J*-*Q* trajectory (a) and *J*-*h* trajectory (b) and influence of crack length (c) and pipe diameter (d) on *J*-*Q* trajectory

In an attempt to clarify the above observations, two effects are distinguished. First, local bending originates from a difference between the centre of the applied force and the centre of the resulting force in the cracked ligament [40]. Second, the presence of axial symmetry in pipe specimens increases the stiffness of the specimens and hence prevents bending.

The first effect is illustrated by examining the stress distribution in the remaining ligament ($b_0 = t - a_0$). Figure 14a indicates that CWP specimens are more susceptible to bending than unpressurized pipe specimens with identical defect dimensions. This bending creates higher stresses near the crack tip and lower stresses at the back side of the crack (near $r/b_0 = 1$). Since the constraint calculations are based on the stress fields' magnitude in the vicinity of the crack tip, the increased constraint in CWP specimens is attributed to an increased bending. This is confirmed by Figure 14b for CWP specimens. Remark a minor discontinuity in the stress field around $r/b_0 = 0.7$. This discontinuity is attributed to the transition between plastic and elastic deformation. On the other hand, the mesh was selected to

obtain an accurate description of the stresses near the crack tip rather than the back side of the crack, resulting in a relatively coarse mesh in this region.

The second effect mainly explains the observed influence of the pipe diameter. Regarding the unpressurized pipe specimens, the centre of the resulting force will, within the investigated range of defect sizes, never shift significantly from the pipe axis. Hence, the constraint trajectories remain relatively independent of the pipes' diameter. In contrast, the CWP specimens lack axial symmetry and are therefore likely to bend more. This bending effect is most pronounced for large diameter pipes, as the absence of curvature decreases the bending stiffness. Consequently, the bending stresses increase and subsequently the constraint.

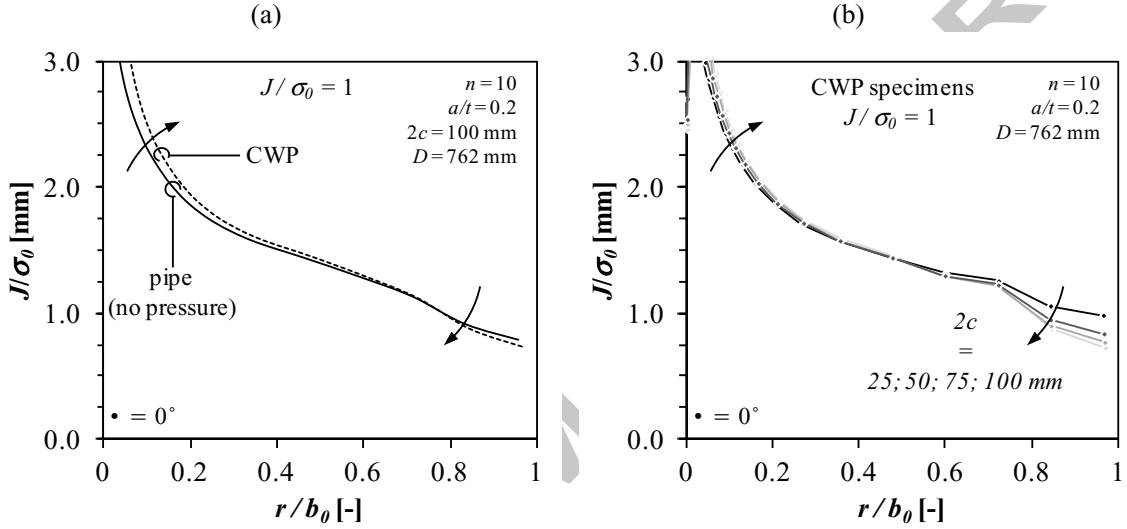

Figure 14: Stress profile in remaining ligament: comparison between CWP and unpressurized pipe (a) and influence of defect length in CWP specimens (b)

In addition to the midpoint of the crack, the constraint is evaluated at the surface ends of the crack. Given the symmetry along the length axis of the specimens, both for the CWP and the pipe specimens, no difference in bending is present that potentially shifts the constraint at the surface end of the crack between both specimen types. Accordingly, it should not surprise that the constraint evolution at these points is very similar for pipe and CWP specimens. By means of example, the *J-Q* trajectories are plotted for specimens with varying initial defect depths (Figure 15a) and defect lengths (Figure 15b).

Based on the above observations and explanations, the apparent fracture toughness obtained through CWP testing is expected to be slightly lower than the toughness obtained from full scale testing. This is in agreement with experimental data published by Cheng et al. [41]. Accordingly, it is concluded that CWP testing slightly underestimates the fracture toughness as compared to the full scale behaviour, especially for large defect sizes and/or large diameter pipes.

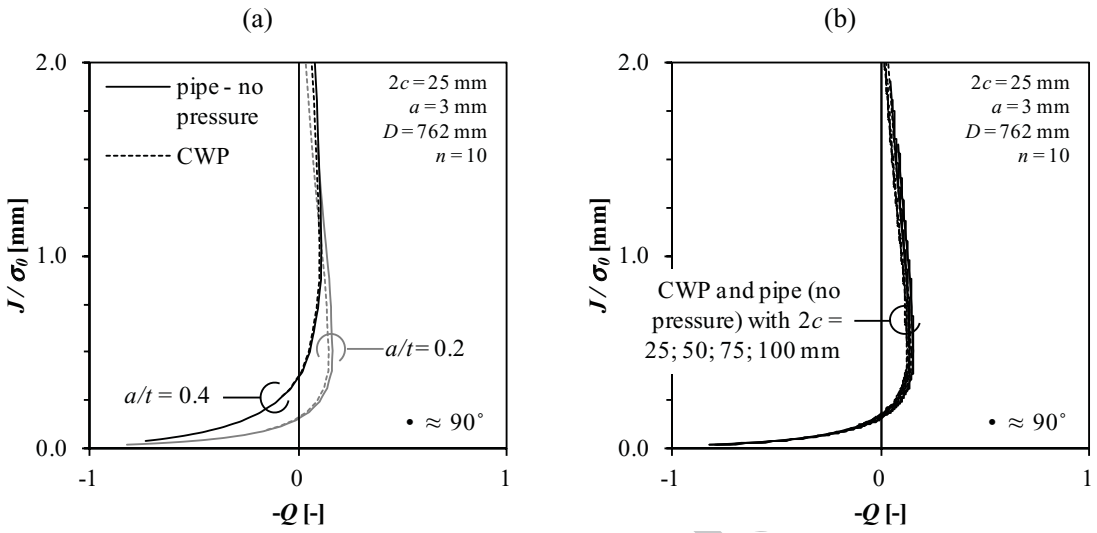

Figure 15: Influence of defect depth (a) and length (b) on constraint evolution at surface end of defect for pipe and CWP specimens

4.4. Influence of weld metal mismatch

The *J-Q* calculations for the weld metal strength mismatched configurations are based on a comparison with the MBL solutions of materials with similar yield strength as the material where the crack is located, i.e. the weld. A similar dependency of the constraint evolution on the mismatch level is observed for all constraint parameters, though only the *J-Q* trajectories are shown in this section. A higher mismatch level (overmatch) results in a decrease of the constraint, whereas a lower mismatch level (undermatch) increases the constraint (Figure 16a). This is understood as, for higher strength weld metals, the plastic zone originating from the crack tip develops more easily in the adjacent softer base material. This plastic deformation results in a relaxation of the stresses near the crack tip, hence the constraint lowers. In contrast, for undermatching welds limited plastic deformation takes place in the adjacent (high strength) base material. Accordingly, the deformation is confined to the weld metal surrounding the crack tip and therefore the hydrostatic stresses increase relative to the evenmatching (homogeneous) situation. The above trend is in agreement with literature [42-44].

The above dependency is most pronounced at higher crack driving force levels. Although valid *Q*-calculations have not always been obtained at low crack driving force levels (ΔQ values exceeding 0.1), the *J-Q* curves are likely to merge at lower crack driving force levels. This observation is understood as the influence of weld metal mismatch only becomes relevant once the plastic zone, developing from the crack tip, reaches the fusion line and interacts with the adjacent base material [44].

Another relevant observation relates to the similarity between the constraint evolution in unpressurized pipe and CWP specimens (Figure 16b). This allows concluding that, for a wide variety of strength mismatch conditions, the CWP specimens remain a slightly conservative alternative to full scale testing.

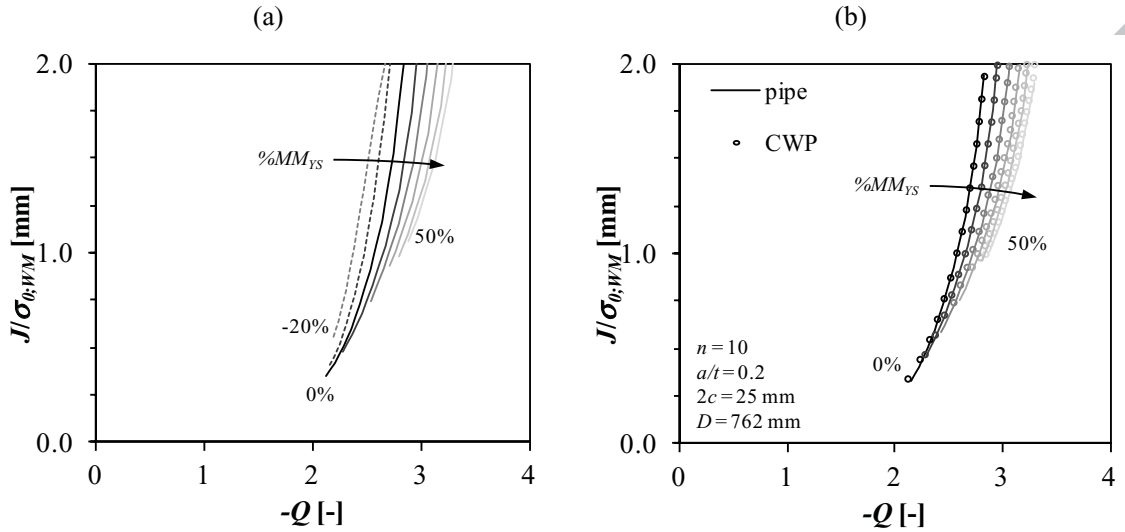

Figure 16: Influence of weld strength mismatch on constraint: influence of mismatch level (a) and comparison between CWP and pipe specimens (b)
with mismatch levels varying in steps of 10% on the materials' yield strength

The weld width is expected to influence the constraint evolution. Focusing on strength overmatch situations, an increasing weld width will shield the crack tip stress fields from the adjacent softer material and it takes longer before the plastic zone reaches the fusion line. Accordingly, the beneficial effect going with strength overmatch is expected to decrease and to be postponed to higher crack driving force levels. Figure 17a shows a comparison between a narrow and wide weld as defined in §3.3. As expected, the wide weld shows less loss of constraint for increasing mismatch levels. This difference is highlighted by comparing the Q-values at a constant load level (Figure 17b). The dependency between strength mismatch and Q is stronger for smaller welds.

(a) (b)

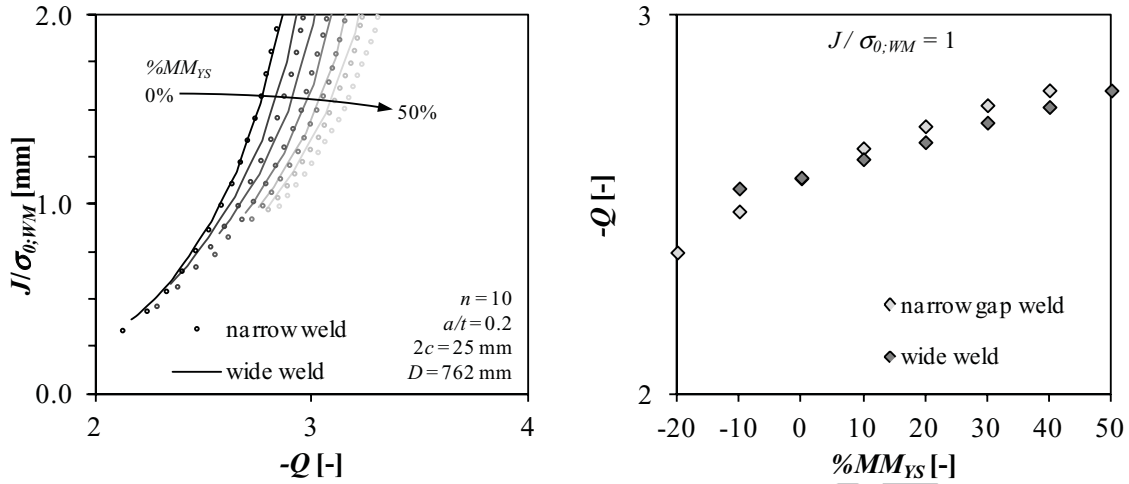

Figure 17: Influence of weld bevel geometry on *J*-*Q* trajectories: global overview (a) and detail at fixed load level $J / \sigma_{0;WM} = 1$ (b)

Bearing in mind that the constraint level relates to the tearing resistance, the following is concluded. Assuming a constant microstructure of the tested specimens an increase of the mismatch level yields a higher tearing resistance. In contrast, undermatching causes a decrease of the tearing resistance.

4.5. Comparison of constraint parameters

In the preceding sections, different parameters have been considered for the evaluation of the constraint ahead of the crack tip. In most cases, these parameters predict similar effects. It is therefore not surprising that these parameters can be uniquely, linearly, related to each other. For the stress triaxiality parameter h and the parameter Q_m, this relationship is approximately independent of the considered specimen type (i.e. pipe or CWP specimen) and loading mode (i.e. with or without internal pressure). The relationship between both parameters however depends on the strain hardening properties of the materials (Figure 18a). More specifically, the strain hardening coefficient n results in a shift of the correlation function. The slope of the correlation remains constant, implying that the constraint loss predicted by both parameters is similar. Moreover, the out-of-plane constraint is captured similarly by both the stress triaxiality h and the Q_m-parameter. Therefore, it is concluded that the observed dependency does not limit the application of either of both parameters in the framework of the presented comparisons as the main aim was to compare different specimen configurations and loading conditions, assuming identical material properties for the different specimens. Hence, the presented results in terms of h or Q_m can be extrapolated to materials with a different strain hardening behavior.

On the contrary, the relationship between the Q-parameter and the stress triaxiality depends on the loading condition, namely the internal pressure (Figure 18b). This is not surprising as the Q-parameter was hardly influenced by the internal pressure level. In contrast to the stress triaxiality, which showed a close to linear dependency on the internal pressure level (§4.2). This difference is attributed to the out-of-plane constraint effects, which are not well captured in case of the Q-parameter. For some applications, this is of minor interest (e.g. cleavage fracture). However, within the current study ductile failure is of primary interest. As it is well known that the out-of-plane constraint influences the material's behavior in this case, preference should therefore be given to a parameter that does account of the out-of-plane effects.

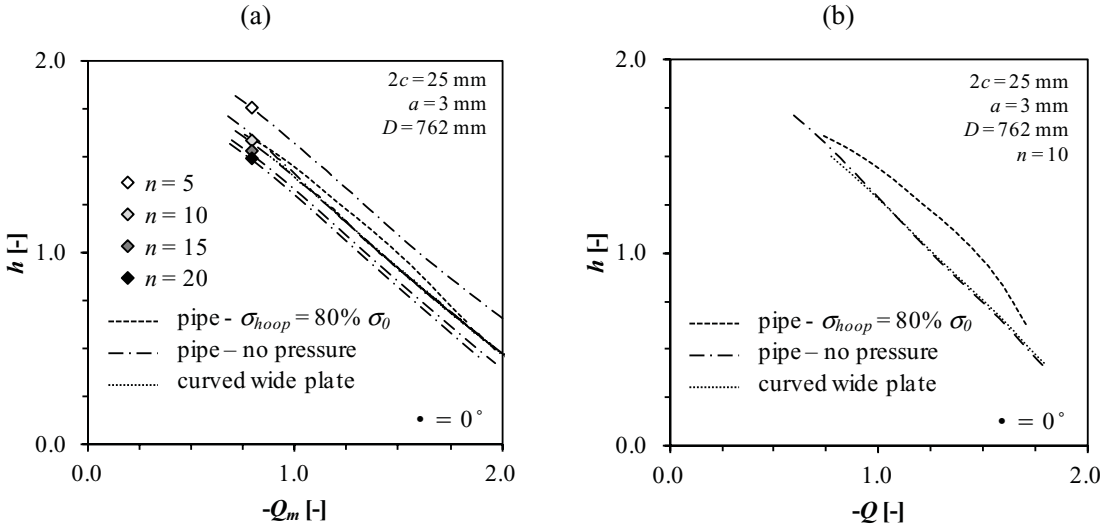

Figure 18: Relation between Q_m and h parameter (a) and Q and h parameter (b)

5. Conclusions

Based on an extensive set of finite element simulations, the crack tip stress fields and resulting *J-Q, J-*Q_m and *J-h* trajectories have been analyzed in (pressurized) pipe and CWP specimens. From these simulations it is concluded that:

- Internal pressure does not affect the in-plane constraint Q, only the out-of-plane constraint is slightly increased with increasing pressure level.
- CWP specimens can be considered to determine the apparent toughness of defected pipes. The constraint evolution in both homogeneous and weld strength mismatched configurations are comparable for pipe and CWP specimens. Although the CWP specimens remain slightly conservative.
- Weld strength mismatch influences the constraint evolution in pipe specimens. Overmatching welds show a higher loss of constraint than evenmatching (homogeneous) and undermatching welds.
- To characterize the constraint in case ductile failure is studied, the Q_m and h parameter appeared equivalent. Contrary, the Q-parameter underestimated the impact of the multi-axial loading conditions.

6. Acknowledgements

The authors would like to acknowledge the financial support of the IWT (Agency for innovation by science and technology – grants nrs. SB-091512 and SB-093512) and the FWO (Research Foundation Flanders – grants nrs. 1.1.880.09.N.00 and 1.1.880.11.N.01).

7. References

1. Jayadevan, K.R., Østby, E. and Thaulow, C. *Fracture response of pipelines subjected to large plastic deformation under tension.* International Journal of Pressure Vessels and Piping 2004; 81: 771-783.
2. Østby, E., Jayadevan, K.R. and Thaulow, C. *Fracture response of pipelines subjected to large plastic deformation under bending*. International Journal of Pressure Vessels and Piping 2005; 82: 201-215.
3. Denys, R. and Lefevre, T.L. *UGent guidelines for Curved Wide Plate testing.* In: Pipeline Technology Conference Ostend, Belgium; 2009, paper n° 2009-110.
4. Denys, R., Andrews, R., Zarea, M. and Knauf, G. *EPRG Tier 2 guidelines for the assessment of defects in transmission pipeline girth welds*. In: International Pipeline Conference Calgary, Alberta, Canada; 2010, paper n° IPC2010-31640.
5. Denys, R., Hertelé, S., Verstraete, M. and De Waele, W. *Strain capacity prediction for strain-based pipeline designs*. In: International Workshop on Welding of High Strength Pipeline Steels Araxá, Brazil; 2011, p.1-13.
6. Verstraete, M., De Waele, W., Denys, R. and Hertelé, S. *Pressure correction factor for strain capacity predictions based on Curved Wide Plate testing*. In: International Pipeline Conference Calgary, Alberta, Canada; 2012, paper n° IPC2012-90592.
7. Denys, R., Hertelé, S., Verstraete, M., De Waele, W., *Strain capacity prediction for strain-based pipeline designs*. In: International Workshop on Welding of High Strength Pipeline Steels, Araxá, Brazil; 2011, p. 1-13.
8. Fairchild, D.P., Kibey, S., Tang, H., Krishnan, V.R., Macia, M.L., Cheng, W. and Wang, X. *Continued advancements regarding capacity prediction of strain-based pipelines*. In: International Pipeline Conference Calgary, Alberta, Canada; 2012, paper n° IPC2012-90471.
9. Al-Ani, A.M. and Hancock, J.W. *J-dominance of short cracks in tension and bending.* Journal of Mechanics and Physics of Solids 1991; 39: 23-43.
10. Betegon, C. and Hancock, J.W. *Two-parameter characterization of elastic-plastic crack tip fields.* Journal of Applied Mechanics 1991; 58: 104-113.
11. Yang, S., Chao, Y.J. and Sutton, M.A. *Higher order asymptotic fields in a power-law hardening material.* Engineering Fracture Mechanics 1993; 45: 1-20.
12. O'Dowd, N.P. and Shih, C.F. *Family of crack-tip fields characterized by triaxiality parameter: Part I - structure of fields.* Journal of Mechanics and Physics of Solids 1991; 39: 989-1015.
13. O'Dowd, N.P. and Shih, C.F. *Family of crack-tip fields characterized by triaxiality parameter: Part II - application.* Journal of Mechanics and Physics of Solids 1992; 40: 939-963.
14. Dodds, R.H., Shih, C.F. and Anderson, T.L. *Continuum and micromechanics treatment of constraint in fracture.* 1993; Office of Nuclear Regulatory Research: report NUREG/CR-5971.
15. Cravero, S., Bravo, R.E. and Ernst, H.A. *Constraint evaluation and effects on J-R resistance curves for pipes under combined load conditions*. In: International Offshore and Polar Engineering Conference, Vancouver, British Columbia, Canada; 2008, p. 149-156.
16. Henry, B.S. and Luxmoore, A.R., *The stress triaxiality constraint and the Q-value as a ductile fracture parameter*. Engineering Fracture Mechanics 1997; 57(4): 375-390.
17. Hebel, J., Hohe, J., Friedmann, V. and Siegele, D., *Experimental and numerical analysis of in-plane and out-of-plane crack tip constraint characterization by secondary fracture parameters*. International Journal of Fracture 2007; 146: 173-188.
18. Yuan, H. and Brocks, W., *Quantification of constraint effects in elastic-plastic crack front fields*. Journal of mechanics and physics of solids 1998; 46(2): 219-241.
19. Kibey, S.A., Lele, S.P., Tang, H., Macia, M.L., Fairchild, D.P., Cheng, W., Noecker, R., Wajutelewicz, P.J., Newbury, B., Kan, W.C. and Cook, M.F. *Full-scale test observations for measurement of tensile strain capacity of welded pipelines*. In: International Offshore and Polar Engineering Conference Maui, Hawaii, USA; 2011, p. 660-667.
20. Hertelé, S., De Waele, W., Denys, R., Verstraete, M. and Van Wittenberghe, J. *Parametric finite element model for large scale tension tests on flawed pipeline girth welds.* Advances in Engineering Software 2012; 47: 24-34.
21. Cravero, S. and Ruggieri, C. *Correlation of fracture behavior in high pressure pipelines with axial flaws using constraint designed test specimens - Part I: plane-strain analyses.* Engineering Fracture Mechanics 2005; 72: 1355-1360.

22. Verstraete, M., De Waele, W., Hertelé, S., Van Minnebruggen, K. and Denys, R.M. *Constraint analysis of Curved Wide Plate specimens.* In: European Conference on Fracture Kazan, Russia; 2012, paper n° ECF19-289.
23. English, S.A. and Arakere, N.K. *Effects of the strain-hardening exponent on two-parameter characterizations of surface-cracks under large-scale yielding.* International Journal of Plasticity 2011; 27: 920-939.
24. Ramberg, W. and Osgood, W.R. *Description of stress-strain curves by three parameters.* 1943; National Advisory Committee for Aeronautics: technical note n° 902.
25. Canadian Standards Association, *CSA Z662 - 11: Oil and gas pipeline systems*. 2011.
26. Ritchie, R.O. and Thompson, A.W. *On macroscopic and microscopic analyses for crack initiation and crack growth toughness in ductile alloys.* Metallurgical Transactions A 1985; 16: 233-248.
27. Brickstad, B. and Sattari-Far, I. *Crack shape developments for LBB applications*. Engineering Fracture Mechanics 2000; 67: 625-646.
28. O'Dowd, N.P. and Shih, C.F., *Two-parameter fracture mechanics theory and applications*. 1992; United States Naval Surface Warfare Center - Carderock Division: London.
29. Ainsworth, R.A., Sattari-Far, I., Sherry, A.H., Hooton, D.G. and Hadley, I., *Methods for including constraint effects within the SINTAP procedures*. Engineering Fracture Mechanics 2000; 67: 563-571.
30. Ranestad, O., Zhang, Z.L. and Thaulow, C. *Quantification of geometry and material mismatch constraint in steel weldments with fusion line cracks.* International Journal of Fracture 1999; 99: 211-237.
31. Pavankumar, T.V., Chattopadhyay, J., Dutta, B.K. and Kushwaha, H.S. *Numerical investigations of crack-tip constraint parameters in two-dimensional geometries.* Pressure Vessels and Piping 2000; 77: 345-355.
32. O'Dowd, N.P. and Shih, C.F. *Two-parameter fracture mechanics: theory and applications.* ASTM STP 1207. Fracture Mechanics, vol. 24. West Conshohocken, PA: ASTM International; 1995. p. 21-47.
33. Denys, R. and Lefevre, A.A., *Failure characterization of a girth weld with surface-breaking flaw under tensile load.* In: Pipeline Technology Conference, Ostend, Belgium; 2009, paper n° 2009-111.
34. Cravero, S., Bravo, R.E. and Ernst, H.A. *Fracture evaluation of cracked pipelines subjected to combined loading*. In: Pipeline Technology Conference Ostend, Belgium; 2009, paper n° 2009-061.
35. Bass, B.R., McAfee, W.J., Williams, P.T. and Pennell, W.E*., Fracture assessment of shallow-flaw cruciform beams tested under uniaxial and biaxial loading conditions*. Nuclear Engineering and Design 1999; 188(3): 259-288.
36. Neimitz, A. and Galkiewicz, J. *Fracture toughness of structural components: influence of constraint.* International Journal of Pressure Vessels and Piping 2006; 83: 42-54
37. Østby, E. and Hellesvik, A.O. *Large-scale experimental investigation of the effect of biaxial loading on the deformation capacity of pipes with defects.* International Journal of Pressure Vessels and Piping 2008; 85: 814-824.
38. Tyson, W.R., Shen, G. and Roy, G. *Effect of biaxial stress on ECA of pipelines under strain-based design.* In: International Offshore and Polar Engineering Conference Lisbon, Portugal; 2007, paper n° ISOPE2007-SBD-01.
39. Shen, G. and Tyson, W.R. *Evaluation of CTOD from J-integral for SE(T) specimens*. In: Pipeline Technology Conference Ostend, Belgium; 2009, paper n° 2009-004.
40. Hertelé, S., De Waele, W. and Denys, R.M. *Development of an analytical reference stress equation for inner-diameter defected curved plates in tension.* International Journal of Pressure Vessels and Piping 2011; 88: 256-261.
41. Cheng, W., Tang, H., Cioielli, P.C., Minnaar, K. and Macia, M.L. *Test methods for characterization of strain capacity: comparison of R-curves from SENT/CWP/FS tests*. In: Pipeline Technology Conference Ostend, Belgium; 2009, paper n° 2009-040.
42. Burstow, M.C., Howard, I.C. and Ainsworth, R.A. *The effects of material strength mismatching on constraint at the limit load of welded three-point bend specimens.* International Journal of Fracture 1998; 89: 117-142.

43. Boothman, D.P., Lee, M.M.K. and Luxmoore, A.R. *The effects of weld mismatch on J-integrals and Q-values for semi-elliptical surface flaws.* Engineering Fracture Mechanics 1999; 64: 433-458.
44. Burstow, M.C., Howard, I.C. and Ainsworth, R.A. *The influence of constraint on crack tip stress fields in strength mismatched welded joints.* Journal of Mechanics and Physics of Solids 1998; 46: 845-872.

1. Jayadevan, K.R., Ostby, E. and Thaulow, C., *Fracture response of pipelines subjected to large plastic deformation under tension.* international journal of pressure vessels and piping, 2004. **81**: p. 771-783.
2. Ostby, E., Jayadevan, K.R. and Thaulow, C., *Fracture response of pipelines subjected to large plastic deformation under bending.* international journal of pressure vessels and piping, 2005. **82**: p. 201-215.
3. Denys, R. and Lefevre, T.L., *UGent guidelines for Curved Wide Plate testing*, in *Pipeline Technology Conference*, 2009, Ostend, Belgium,
4. Denys, R., Andrews, R., Zarea, M. and Knauf, G., *EPRG Tier 2 guidelines for the assessment of defects in transmission pipeline girth welds*, in *International Pipeline Conference*, 2010, Calgary, Alberta, Canada,
5. Denys, R., Hertelé, S., Verstraete, M. and De Waele, W., *Strain capacity prediction for strain-based pipeline designs*, in *International Workshop on Welding of High Strength Pipeline Steels*, 2011, Araxá, Brazil,
6. Verstraete, M., De Waele, W., Denys, R. and Hertelé, S., *Pressure correction factor for strain capacity predictions based on Curved Wide Plate testing*, in *International Pipeline Conference*, 2012, Calgary, Canada,
7. Denys, R., Hertelé, S., Verstraete, M. and De Waele, W. *Strain capacity prediction for strain-based pipeline designs*. in *International Workshop on Welding of High Strength Pipeline Steels*. 2011. Araxá, Brazil.
8. Fairchild, D.P., Kibey, S., Tang, H., Krishnan, V.R., Macia, M.L., Cheng, W. and Wang, X., *Continued advancements regarding capacity prediction of strain-based pipelines*, in *International Pipeline Conference*, 2012, Calgary, Alberta, Canada, IPC2012-90471.
9. Al-Ani, A.M. and Hancock, J.W., *J-dominance of short cracks in tension and bending.* Journal of mechanics and physics of solids, 1991. **39**: p. 23-43.
10. Betegon, C. and Hancock, J.W., *Two-parameter characterization of elastic-plastic crack tip fields.* ASME journal of applied mechanics, 1991. **58**: p. 104-113.
11. Yang, S., Chao, Y.J. and Sutton, M.A., *Higher order asymptotic fields in a power-law hardening material.* Engineering Fracture Mechanics, 1993. **45**: p. 1-20.
12. O'Dowd, N.P. and Shih, C.F., *Family of crack-tip fields characterized by triaxiality parameter: Part I - structure of fields.* Journal of Mechanics and Physics of Solids, 1991. **39**(8): p. 989-1015.
13. O'Dowd, N.P. and Shih, C.F., *Family of crack-tip fields characterized by triaxiality parameter: Part II - application.* Journal of Mechanics and Physics of Solids, 1992. **40**(5): p. 939-963.
14. Dodds, R.H., Shih, C.F. and Anderson, T.L., *Continuum and micromechanics treatment of constraint in fracture*. 1993, Office of nuclear regulatory research.
15. Cravero, S., Bravo, R.E. and Ernst, H.A. *Constraint evaluation and effects on J-R resistancecurves for pipes under combined load conditions*. in *International Offshore and Polar Engineering Conference*. 2008. Vancouver, British Columbia, Canada.
16. Henry, B.S. and Luxmoore, A.R., *The stress triaxiality constraint and the Q-value as a ductile fracture parameter.* Engineering Fracture Mechanics, 1997. **57**(4): p. 375-390.
17. Hebel, J., Hohe, J., Friedmann, V. and Siegele, D., *Experimental and numerical analysis of in-plane and out-of-plane crack tip constraint characterization by secondary fracture parameters.* International Journal of Fracture, 2007. **146**: p. 173-188.
18. Yuan, H. and Brocks, W., *Quantification of constraint effects in elastic-plastic crack front fields.* Journal of mechanics and physics of solids, 1998. **46**(2): p. 219-241.
19. Kibey, S.A., Lele, S.P., Tang, H., Macia, M.L., Fairchild, D.P., Cheng, W., Noecker, R., Wajutelewicz, P.J., Newbury, B., Kan, W.C. and Cook, M.F., *Full-scale test observations for measurement of tensile strain capacity of welded pipelines*, in *International Offshore and Polar Engineering Conference*, 2011, Maui, Hawaii, USA,

20. Hertelé, S., De Waele, W., Denys, R., Verstraete, M. and Van Wittenberghe, J., *Parametric finite element model for large scale tension tests on flawed pipeline girth welds.* Advances in Engineering Software, 2012. **47**(1): p. 24-34.
21. Cravero, S. and Ruggieri, C., *Correlation of fracture behavior in high pressure pipelines with axial flaws using constraint designed test specimens - Part I: plane-strain analyses.* Engineering Fracture Mechanics, 2005. **72**: p. 1355-1360.
22. Verstraete, M., De Waele, W., Hertelé, S., Van Minnebruggen, K. and Denys, R.M., *Constraint analysis of Curved Wide Plate specimens*, in *European Conference on Fracture*, 2012, Kazan, Russia,
23. English, S.A. and Arakere, N.K., *Effects of the strain-hardening exponent on two-parameter characterizations of surface-cracks under large-scale yielding.* International journal of plasticity, 2011. **27**: p. 920-939.
24. Ramberg, W. and Osgood, W.R., *Description of stress-strain curves by three parameters*. 1943, National Advisory Committee for Aeronautics: Washington.
25. CSA, *Z662 - 11: Oil and gas pipeline systems*. 2011.
26. Ritchie, R.O. and Thompson, A.W., *On macroscopic and microscopic analyses for crack initiation and crack growth toughness in ductile alloys.* Metallurgical Transactions A, 1985. **16**: p. 233-248.
27. Brickstad, B. and Sattari-Far, I., *Crack shape developments for LBB applications.* Engineering Fracture Mechanics, 2000. **67**(6): p. 625-646.
28. O'Dowd, N.P. and Shih, C.F., *Two-parameter fracture mechanics theory and applications*. 1992, United States Naval Surface Warfare Center - Carderock Division: London.
29. Ainsworth, R.A., Sattari-Far, I., Sherry, A.H., Hooton, D.G. and Hadley, I., *Methods for including constraint effects within the SINTAP procedures.* Engineering Fracture Mechanics, 2000. **67**: p. 563-571.
30. Ranestad, O., Zhang, Z.L. and Thaulow, C., *Quantification of geometry and material mismatch constraint in steel weldments with fusion line cracks.* International journal of fracture, 1999. **99**: p. 211-237.
31. Pavankumar, T.V., Chattopadhyay, J., Dutta, B.K. and Kushwaha, H.S., *Numerical investigations of crack-tip constraint parameters in two-dimensional geometries.* Pressure Vessels and Piping, 2000. **77**: p. 345-355.
32. O'Dowd, N.P. and Shih, C.F., *Two-parameter fracture mechanics: theory and applications*. Standard Technical Publication 1207, ed. ASTM. 1995. 21-47.
33. Denys, R. and Lefevre, A.A., *Failure characterization of a girth weld with surface-breaking flaw under tensile load*, in *Pipeline Technology Conference*, 2009, Ostend, Belgium, Ostend2009-111.
34. Cravero, S., Bravo, R.E. and Ernst, H.A., *Fracture evaluation of cracked pipelines subjected to combined loading*, in *Pipeline technology conference*, 2009, Ostend, Belgium,
35. Bass, B.R., McAfee, W.J., Williams, P.T. and Pennell, W.E., *Fracture assessment of shallow-flaw cruciform beams tested under uniaxial and biaxial loading conditions.* Nuclear Engineering and Design, 1999. **188**(3): p. 259-288.
36. Neimitz, A. and Galkiewicz, J., *Fracture toughness of structural components: influence of constraint.* International Journal of Pressure Vessels and Piping, 2006. **83**(1): p. 42-54.
37. Ostby, E. and Hellesvik, A.O., *Large-scale experimental investigation of the effect of biaxial loading on the deformation capacity of pipes with defects.* international journal of pressure vessels and piping, 2008. **85**: p. 814-824.
38. Tyson, W.R., Shen, G. and Roy, G., *Effect of biaxial stress on ECA of pipelines under strain-based design*, in *International offshore and polar engineering conference*, 2007, Lisbon, Portugal,
39. Shen, G. and Tyson, W.R., *Evaluation of CTOD from J-integral for SE(T) specimens*, in *Pipeline Technology Conference*, 2009, Ostend, Belgium,

40. Hertelé, S., De Waele, W. and Denys, R.M., *Development of an analytical reference stress equation for inner-diameter defected curved plates in tension.* international journal of pressure vessels and piping, 2011(88): p. 256-261.
41. Cheng, W., Tang, H., Cioielli, P.C., Minnaar, K. and Macia, M.L., *Test methods for characterization of strain capacity: comparison of R-curves from SENT/CWP/FS tests*, in *Pipeline Technology Conference*, 2009, Ostend, Belgium,
42. Burstow, M.C., Howard, I.C. and Ainsworth, R.A., *The effects of material strength mismatching on constraint at the limit load of welded three-point bend specimens.* International journal of fracture, 1998. **89**: p. 117-142.
43. Boothman, D.P., Lee, M.M.K. and Luxmoore, A.R., *The effects of weld mismatch on J-integrals and Q-values for semi-elliptical surface flaws.* Engineering Fracture Mechanics, 1999. **64**: p. 433-458.
44. Burstow, M.C., Howard, I.C. and Ainsworth, R.A., *The influence of constraint on crack tip stress fields in strength mismatched welded joints.* Journal of mechanics and physics of solids, 1998. **46**(5): p. 845-872.